NUMERICAL OPTIMIZATION OF THE TONAL NOISE OF A BACKWARD CENTRIFUGAL FAN USING A FLOW OBSTRUCTION

Franck PEROT[1], Min-Suk KIM[1], Vincent LEGOFF[2],
Xavier CARNIEL[3], Yvon GOTH[3], Christian CHASSAIGNON[4]

[1]*EXA, Aeroacoustics Applications, 150 North Hill Drive, CA, 94005, USA*

[2] *EUROXA, 76 route de la demi-lune, 92057 Paris La Défense, France*

[3]*CETIM, 52, avenue Félix-Louat, BP 80064, 60300 Senlis, France*

[4]*DYVA, 10 rue Maryse Bastié, 69008Lyon, France*

SUMMARY

This paper focuses on a passive noise control device so-called flow obstruction reducing the fan BPF noise. The obstruction is located upstream of a radial fan with a heat exchanger placed in between. Some measurements performed at various operating conditions show that for an optimal position and orientation of the obstruction, the blade passing frequency noise is reduced by 10-13 dB. The goal of this paper is to use a CFD/CAA approach for modeling this problem and numerically determine the optimized position of the obstruction. Simulations results are also used to provide a better understanding of the physical mechanisms involved in the noise reduction.

INTRODUCTION

Broadband and particularly tonal content of the noise radiated by fans can be perceived as a strong annoyance for people staying in their vicinity and can affect working conditions of operators. As a consequence, fan noise reduction represents a real challenge and an important business criterion for fan and integrated system suppliers. The origin of tonal noise is mainly related to the uniformity and unsteadiness of the inlet flow and to rotor-casing interactions. Tonal noise occurs at the Blade Passing Frequency f_0 (BPF) and sub-harmonics $2.f_0$, $4.f_0$,… which frequency values depend on the rotation frequency and the number of blades of the fan.

In this study, our interest is focused on the effect of a passive noise control device so-called flow obstruction significantly reducing the fan BPF noise and having little effect on the broadband content [1]. This device is calibrated in such a way that the shape, position and orientation with respect to the fan are optimized. The obstruction is located upstream of a centrifugal fan with a heat exchanger placed in between in order to load the fan as in realistic hood conditions. Some

measurements performed at various operating conditions on the CETIM fan aeroacoustics test bench show that for an optimal position and orientation of the obstruction, the BPF noise is reduced by 10-13 dB [2].

The main goal of this paper is to use a CFD/CAA approach for fully modeling this problem and for capturing the noise reduction mechanism induced by the obstruction. Considering the time and cost associated with the testing procedure, a validated digital approach for optimizing obstruction designs and positions could be offered as a valuable alternative to fan suppliers and engineers which goal is to improve acoustics performances during the development stages. Simulations results are also used to provide a better understanding of the physical mechanisms involved in the noise reduction. The CFD/CAA code PowerFLOW 4.3 based on the Lattice Boltzmann Method (LBM) is used [3,4,5]. This flow and acoustics solver is transient, explicit and compressible and the full fan and bench geometries are included in the simulation domain. The fan is truly rotating during the simulation using a Local Reference Frame (LRF) approach [6,7,8]. The flow-induced noise contribution radiated from the turbulent flow is simulated during the transient flow simulation and no coupling to another acoustics propagator solver is required [9,10,11]. Validation simulations are carried out at three conditions and various obstruction positions to validate the fan noise predictions and the effects of the heat exchanger and flow obstruction. Additional simulations are also performed at different obstruction positions and orientations in order to check that the simulations can efficiently be used to optimize the obstruction location. Additional post-processing of the transient flow and acoustics fields are used to show the effect of the obstruction on the radiated noise. In particular, the mean and transient blade pressure repartition and the radiated acoustics patterns investigated.

EXPERIMENTS OVERVIEW

Experimental setup

The 6-blade backward centrifugal fan studied in this paper is shown in Figure 1 and is productively used to cool heavy-duty machine engines. The fan is mounted on the CETIM fan aeroacoustics bench in order to provide a detailed aeroacoustics characterization under different conditions [2].During the measurements, the fan revolution speed is imposed and the mass flow measured at the outlet of the bench. Three configurations are tested:

- Conf. A: Fan without heat exchanger (Figure 2 - left)
- Conf. B: Fan with heat exchanger
- Conf. C: Fan with heat exchanger and with obstruction (Figure 2 - right)

For each configuration, measurements are performed at 1800 rpm and 2200 rpm, this latter value being defined as the nominal operating condition. For configuration A, the fan operating point is kept approximately the same as conf. B and C by adding a pressure loss into the system in order to compensate for the pressure loss of the heat exchanger present in conf. B and C. This additional pressure loss takes the form of a calibrated orifice added at the outlet of the system. For conf. C, the center of the obstruction is aligned with the center of rotation of the fan. The angular position and the distance from the obstruction to the heat exchanger are controlled by using a motorized rotating system and by adjusting the distance of this system to the heat exchanger, respectively. For most of the experiments discussed in this paper, the distance exchanger-obstruction is fixed to 20 mm. Noise measurements are performed at five microphones located upstream the fan as shown in Figure 2.

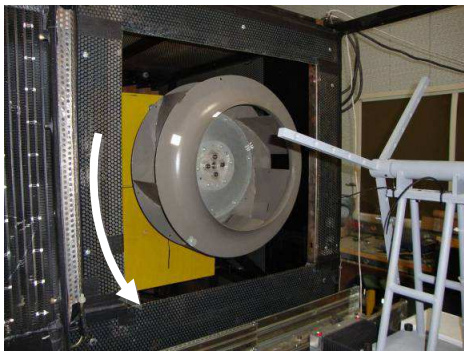

Figure 1: 6-bladecentrifugal fan mounted on the CETIM aeroacoustics bench

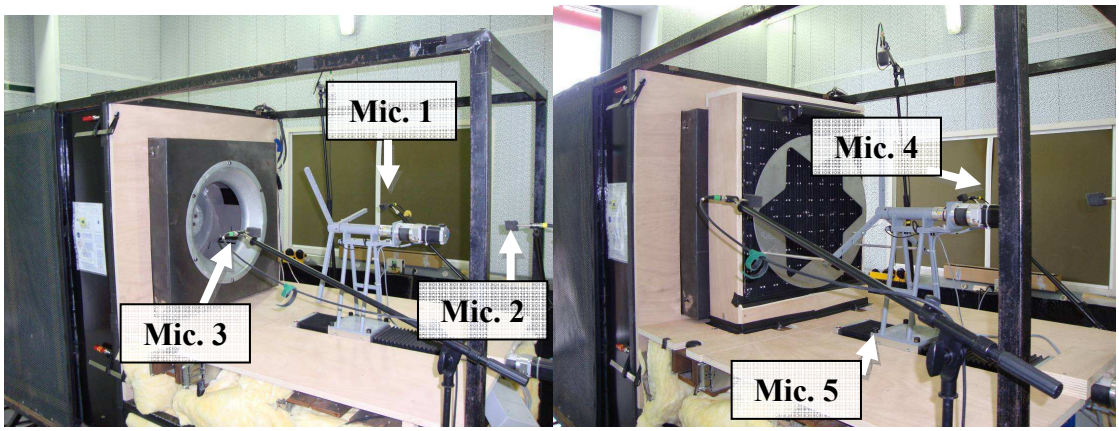

Figure 2: Pictures of the experimental setup: Conf. A (left); Conf. C (Right)

Results overview

SPLs corresponding to the three configurations at 2200 rpm are represented in Figure 3. For conf. C, the optimal position of the obstruction is shown. The BPF $f_0=rpm.N_{blade}/60=220$ Hz is present for configurations A and B and is, as expected, significantly reduced for conf. C. Two frequencies are visible only for conf. A at 160 Hz and 240 Hz and seems to be related to standing modes of the bench which intensities are enhanced by the presence of the outlet diaphragm used to adjust the mass flow rate. From the SPL measured at microphones 1,2,3 and 4 the acoustic power in the range [10-1000 Hz] is calculated: $L_{w,A}$= 103.2 W; $L_{w,B}$= 98.2 W; $L_{w,A\_nopeaks}$ = 98.4 W (peaks at 160 Hz and 240 Hz have been manually removed for Conf. A). As a consequence, with an operating point kept constant and with a relatively smooth incoming flow, the heat exchanger has not a significant effect on fan noise. The main difference between conf. B and C concerns the BPF and only slight differences are observed on sub-harmonics and broadband content.

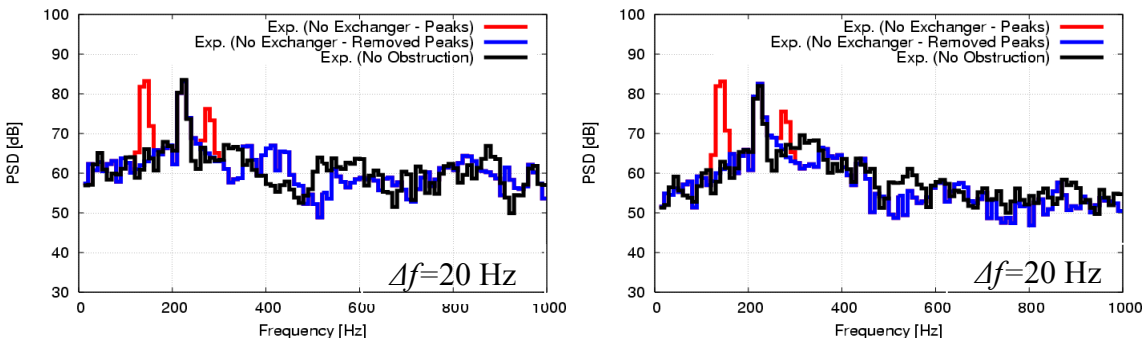

Figure 3: SPL at MIc. 1 (left) and 2 (right) for Conf. A (red); Conf. B (black) and Conf. A – 160 Hz and 240 Hz peaks removed (blue).

The effect of the obstruction angle for conf. C is shown in Figure 4 for which the SPL (Δf=1 Hz) corresponding to the optimal obstruction angle is represented in blue. Confirming the observations

made from Figure 3, the obstruction angle mainly affects the BPF and, at the optimal position (Conf. C_{opt}), the BPF level is almost the same as the broadband one. By varying the angle by 3° and 15° an increase of 6 dB and 13 dB is observed, respectively.

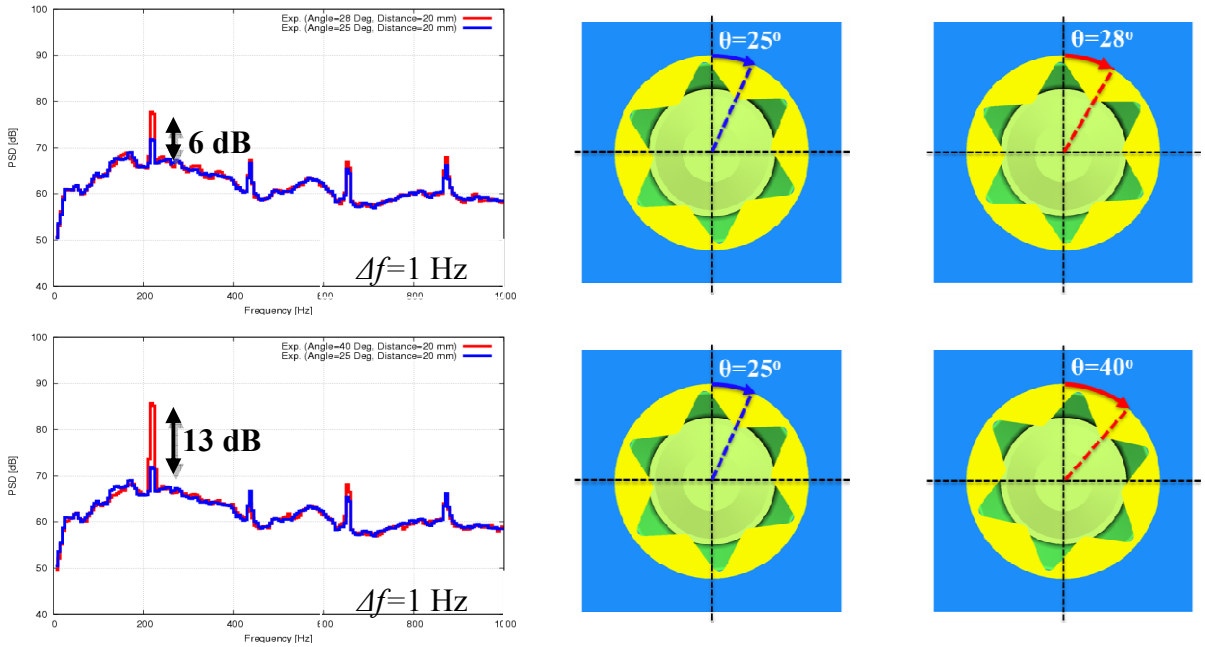

Figure 4: Effect of the obstruction angle on the SPL measured at Mic.1.
Top: optimal position; Bottom: worse position providing quasi same results as Conf. B.

NUMERICAL APPROACH

Lattice Boltzmann Method

The CFD/CAA code PowerFLOW 4.3 is used to compute unsteady flow physics. The code is based on the Lattice Boltzmann Method (LBM). Lattice based methods were proposed a couple of decades ago [12] as an alternative numerical method to traditional Computational Fluid Dynamics (CFD). Unlike conventional methods based on discretizing the macroscopic continuum equations, LBM starts from "mesoscopic" kinetic equations, i.e. the Boltzmann equation, to predict macroscopic fluid dynamics. The current approach is called VLES and includes an advanced turbulent wall-model taking into account for pressure gradients. More details on the method can be found in [13-19].

For simulations of flow with arbitrary geometry rotating in time around a fixed axis, the 3-D dimensional computational domain can be divided into an inner and an outer domain. The inner domain has a grid fixed with the rotating geometry so that the geometry does not have a relative motion with respect to the grid. This forms a "body-fixed" Local Reference Frame (LRF) domain with the rotating geometry. The grid in the outer domain is fixed with the ground and forms a "ground-fixed" reference frame domain [20,21]. Between the inner domain and outer domain, there is a closed transparent interface to connect fluid flows. The basic Lattice Boltzmann concept and algorithm for solving fluid flows across different reference frames was formulated by Chen [22] and Hoch [23].Examples of application can be found in [4,5,6,7,8,25,26].

Numerical Modeling

The entire bench and the three different configurations (Figure 5) are modeled in the simulation including as much details as available. Similarly to the real setup, the digital bench is located inside a large plenum (not represented) for which the ambient atmospheric pressure p_0=101325 Pa is constant. All the surfaces are defined as rigid walls without taking into account for the real

materials properties (absorption and vibrations). The heat exchanger is modeled as a porous medium which pressure loss is defined as a function of the mass flow and derived from the performance curve of the real exchanger. During the simulation, only the fan rotation speed is imposed (2200 rpm) and the system finds its equilibrium, *i.e.* the room pressure increases, the exchanger pressure adjusts with respect to the instantaneous mass flow passing through and the mass flow measured at the outlet duct converges. The Variable Resolution (VR) scheme is plotted in Figure 6 and is applied to the entire simulations. The VR10 represented in light blue corresponds to a resolution of Δx=1 mm and to a 6 cells blade offset. For each VR*i* region, the resolution is $\Delta xi=2^i.\Delta x$. Two setups are used, a "fine" one including VR10 and a coarser one for which VR10 is removed and the finer resolution is then Δx=2mm. At the microphone locations, the resolution is Δx_{mic}= 4mm and assuming that the required number of points per wavelength to accurately capture acoustic waves is N_{ppw}=16, the maximum frequency f_{max} this grid solves at the microphones is about:

$$f_{\max} \sim \frac{c_0}{N_{ppw}\Delta x_{mic}} \sim 10.4kHz$$

The simulation time step is dt=5x10^{-6} s for the 1mm simulations and dt=1x10^{-5} s for the 2 mm ones. The simulations are performed on a 216 cores clusters (one calculation node is composed of a twelve cores 2.8 GHz Intel Xeon processors) with Infiniband interconnection. One fan revolution corresponding to T=0.027s is simulated in 320 CPU-h for the 1mm cases and in 160 CPU-h for the 2 mm ones.

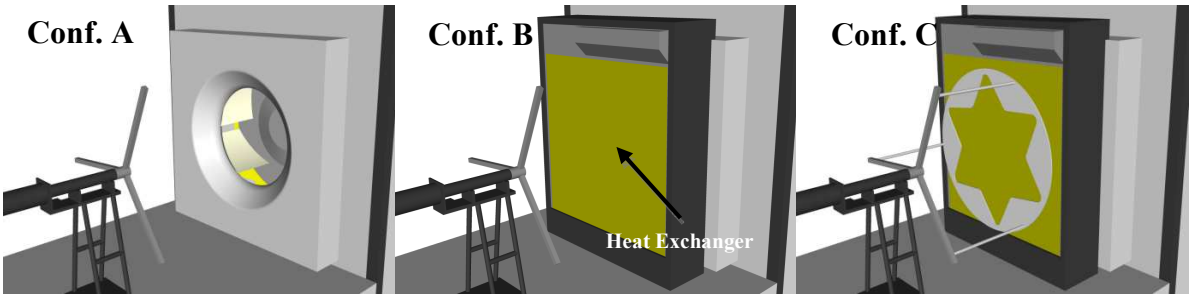

Figure 5: Representation of the three simulated configurations.

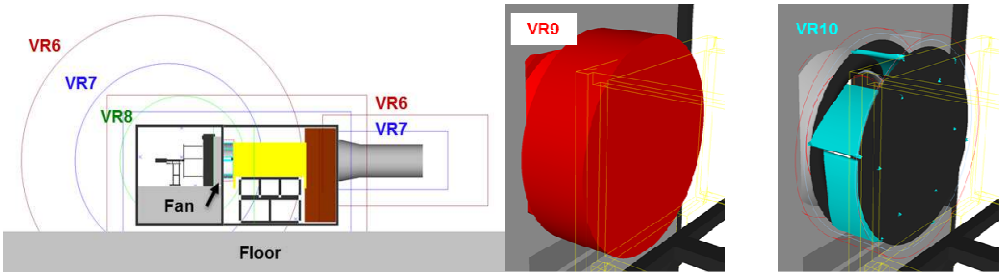

Figure 6: Representation of the resolution scheme used for all the simulations.

Convergence study

In order to assess on the convergence time, 1mm simulations are performed for each configuration over 25 full rotations of the fan. As seen in Figure 7 for configuration A, the convergence of the mass flow is obtained after t=0.2 s of physical time (about 7 revolutions) and the prediction is 1% below the measurement showing a very good agreement. The same simulation, but removing VR10, is performed indicating the same convergence time and an underestimation of the mass flow rate by 6% with respect to the experiments. The same convergence and resolution study performed for conf. B and C leads to the same observation: with a 2mm resolution, the mass flow is underestimated by 5-6% and the convergence obtained after 7 revolutions. An identical analysis

is applied to the SPL calculated from the microphones highlighting the same conclusions (Figure 8). As a consequence, in the rest of the paper, 2 mm simulations are used and 15 revolutions are simulated. The total calculation time for each calculation is then 2400 CPU-h and the restitution time about 11 hours.

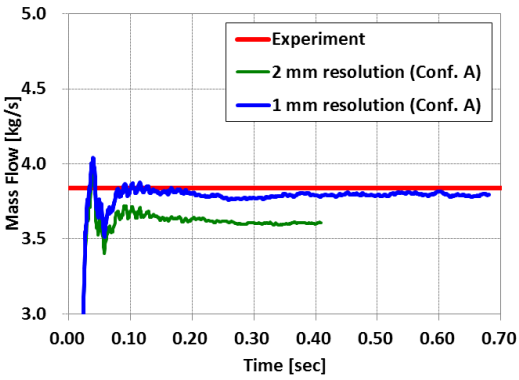

Figure 7: Mass flow convergence and resolution effect for conf. A.

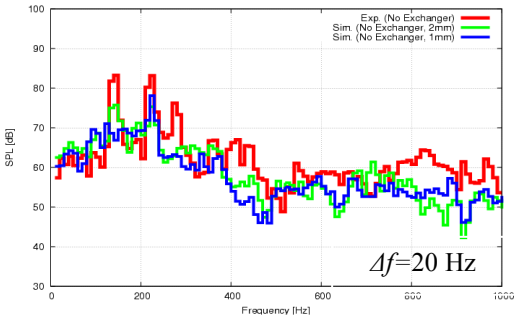

Figure 8:Sound Pressure Levels at Mic. 1 (left) and Mic. 2 (right) for conf. A. Red: Experiments; Blue: Simulation – Δx=1mm; Green: Simulation – Δx=2mm.

RESULTS ANALYSES

Transient flow

Instantaneous vorticity fields are represented in Figure 9 in a *x*-aligned plane passing through the center of the fan for configurations A, B, C and C_{opt}. Without heat exchanger the flow is attached onto the blades and the main source of vorticity comes from the wake of the trailing edges. Higher velocity and turbulence levels are visible with the heat exchanger and a blade-to-blade interaction mechanism seems to be occurring. The effect of the obstruction, for any angles, is to introduce additional fluctuations generated from the 6-petals patterns and convected in direction to the fan. These fluctuations interact with the leading edge of the blades and the resulting flow is more turbulent. Some surface streamlines and near-wall velocity visualizations seem to indicate that the flow is still attached for configurations B and C. Similar and ongoing studies performed on axial fans seem to lead to the same conclusions [27].

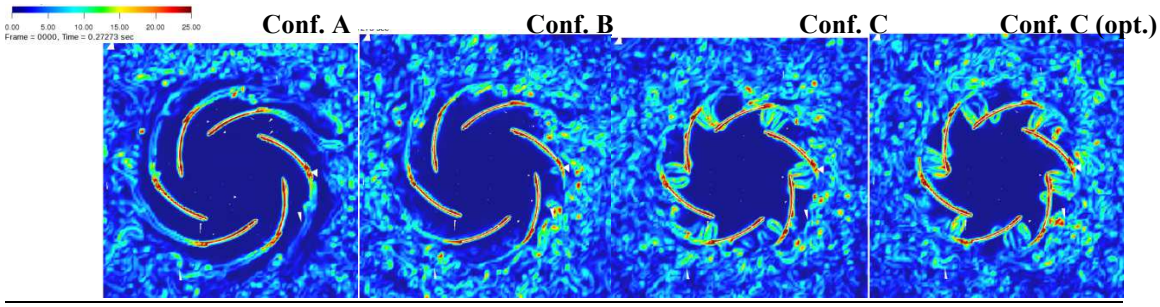

Figure 9:Instantaneous vorticity fields represented in a x-aligned plane passing through the center of the fan.

Radiated noise

Sound Pressure Levels for the three configurations at Mic. 1 and 2 are plotted in Figure10. Since the simulation time used to calculate the SPL is relatively short (t=0.2 s), the bandwidth used is Δf=20 Hz and the SPLs look then less peaky compare to Figure 4. In particular the sub-harmonics are no more visible. This spectral resolution is however sufficient to represent the BPF peak which is here the main topic of interest. It should also be mentioned that the BPF peak level is

independent with the bandwidth chosen when plotting SPL the latter not being true when representing Pressure Spectral Density (PSD) defined as $PSD=SPL/\Delta f$.

In overall, satisfying comparisons are observed for all configurations and microphones. Broadband contents have comparable levels and the BPF peak accurately varies and depends on the configuration. In particular, the BPF sensitivity to the obstruction angle is well-captured between a non optimal (C) and an optimal (C_{opt}) position. A low frequency contribution from 100 Hz to 200 Hz is observed for configuration C on the predicted SPL. Its origin is under investigation and can be due either to the heat exchanger modeling or to noise radiated from the outlet duct and reaching the microphones.

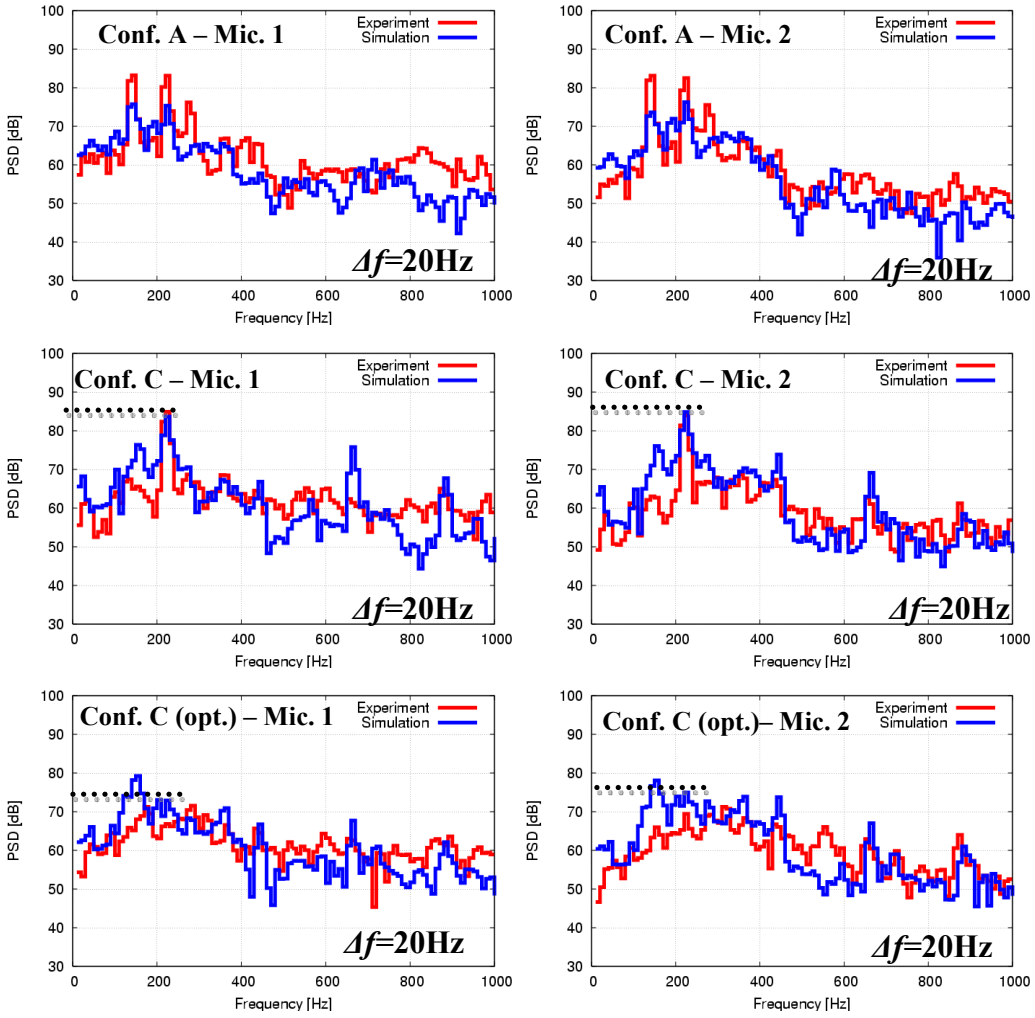

Figure 10: Sound Pressure Levels at Mic. 1 (left) and Mic. 2 (right) for Conf. A, C and C_{opt}. Red: Experiments; Blue: Simulation – $\Delta x=2$ mm.

In Figure 11, the BPF peak level is reported for configuration C for different obstruction orientations. It can be seen that the BPF radiation is not symmetric and varies with the microphone location. In the simulations, an optimal orientation of the obstruction is accurately found and the correct dependency of the peak level with the obstruction recovered. The reference angle chosen both for the experiments and for the simulation is their optimal angles. When using the same absolute angle as a reference, a shift by 8-10 degrees is observed between the simulations and the experiments. The origin of this shift is under investigation and might be related to the effect of absorbing and non-fully reflecting materials used to build the bench or to small geometrical details not taken into account in the simulations. Moreover, sensitivity to the experimental setup has also been observed experimentally.

The BPF peak acoustic power is plotted in Figure 12. This representation reduces directivity effects and shows an even better comparison to experiments indicating that the CFD/CAA simulations can be used as an effective tool for studying and quantifying the effect of obstructions on the BPF noise.

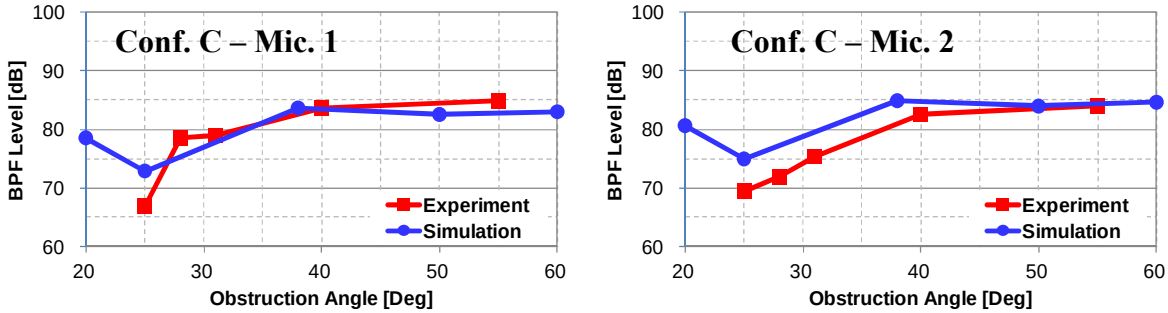

Figure 11: BPF peak levels extracted from SPLs at Mic.1 (left) and Mic.2 (right) at different obstruction angles.

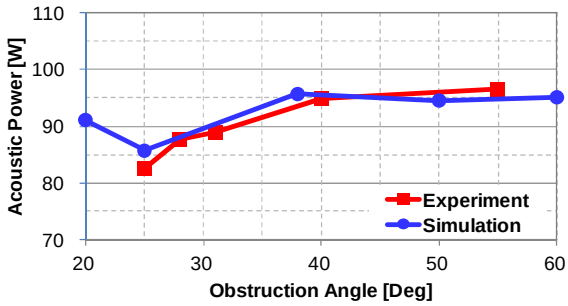

Figure 12: BPF acoustic power vs. obstruction angle. Red: experiments; Blue: simulation.

In Figure 13, the pressure fluctuations in decibels filtered around the BPF are represented on *y*- and *z*-aligned planes for configuration B and Cs (representations so-called "dB-maps"). The main effect of the obstruction positioned in its optimal position is to reduce the intensity in all directions and does not affect the directivity of the noise. In the *(x,y)* plane, the radiation is almost monopolar whereas in the *(x,z)* plane the diffraction effects from the floor is visible. It can also be noticed that the BPF radiates more in direction of the ground and is not axisymmetric. Further investigation on the BPF radiation is proposed in the following section.

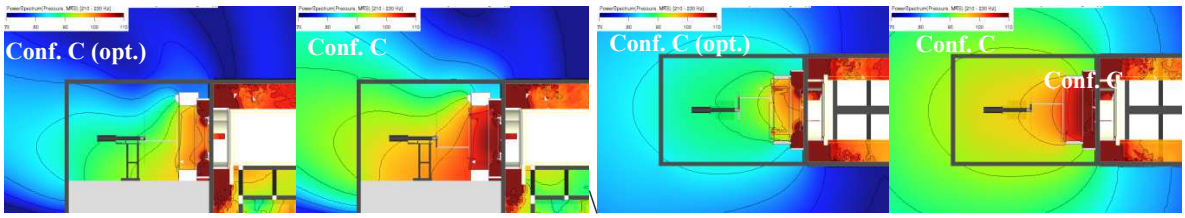

Figure 13:Pressure fluctuations filtered around the BPF represented in dB for configuration B (top) and configuration C at the optimal position and a non-efficient position (bottom).

Investigation on the origins of the noise reduction

In the previous section, it was shown that CFD/CAA simulations can be used to determine an optimal position of the obstruction. In this section, the transient information obtained from the CFD/CAA calculations are used to get an insight on the origins of the noise reduction mechanism already discussed in previous studies[28,29,30].

In Figure 14, instantaneous pressure fluctuations filtered around the BPF from 210 Hz to 230 Hz are represented in a *z*-plane passing through the center of rotation of the fan. These images,

together with the visualization of time animations, show that the noise is generated in the fan area and propagates in direction to the obstruction. No diffraction effects from the obstruction are visible and no additional sources of noise seem to be introduced by the obstruction. The characteristic size of the obstruction being about 30cm and the wavelength λ at 220Hz being λ~1.5m, the obstruction can be considered as acoustically transparent and the previous observation seems to be reasonable. This result could indicate that, instead of having an acoustics effect by itself, the obstruction would mainly modify the flow topology and would modify the flow-induced noise sources in the vicinity of the blades and/or fan.

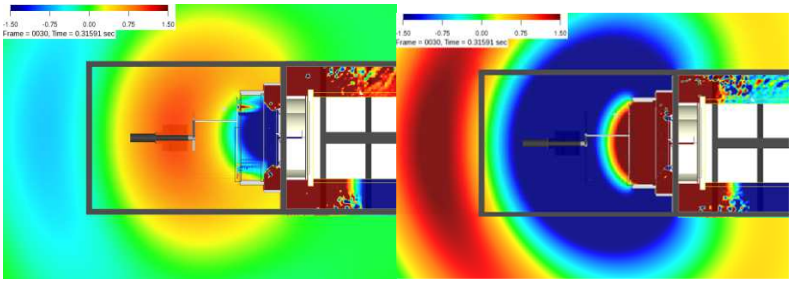

Figure 14: Instantaneous pressure fluctuations filtered around the BPF for configuration C at the optimal position (left) and a non-efficient position (right).

Pressure dB-maps at the BPF are plotted in Figure 15 at the surface of the fan and on the convergent for configurations B, C and C_{opt}. An increase of the pressure fluctuations on the blade is observed both for configurations C and C_{opt} showing a strong, but similar, modification of the flow due to the obstruction (also visible in Figure 9). At the surface of the convergent, a 6-spots pattern is observed for configurations B and C and disappears for configuration C_{opt}. Additional flow investigations (Figure 16a and 16b) show that this pattern is likely related to non-axisymmetric steady vorticity tubes attached onto the convergent and ingested into the fan area.

The previous observations provide a preliminary explanation to the BPF noise reduction mechanism related to this centrifugal fan: during their rotation, the blades periodically breakdown steady structures generating strong pressure fluctuations. Since the location of the tubes is stationary in time and space, the periodic blades passage induce a periodic signal occurring at the BPF. When introducing the obstruction into the system, some coherent structures are generated from the branches of the obstruction and are convected in direction to the fan (Figure 16c and 16d) to finally interact with the structures at the surface of the convergent. When the obstruction and the convergent structures are spatially in opposition of phase, they add-up forming a quasi-axisymmetric tube of vorticity. As a consequence, for configuration C_{opt}, the blades do not breakdown steady vortices but a “continuous curtain” of fluctuations (Figure 16b) which is, apparently, a less efficient source of noise. When the obstruction is not in an optimal position, the various structures do not add-up in a coherent manner and the blades face discrete structures (Figure 16a) and the BPF noise is much intense. This hypothesis has to be further investigated and validated with additional analyses.

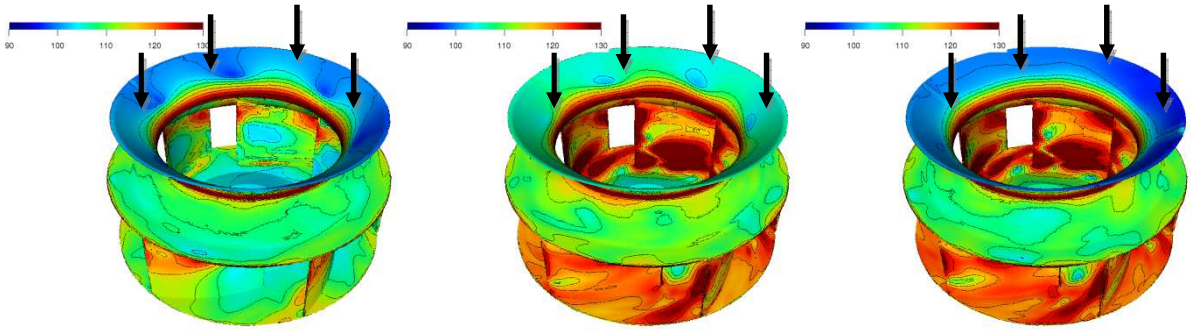

Figure 15: Pressure dB-maps around the BPF represented in dB for configuration B, C and Copt.

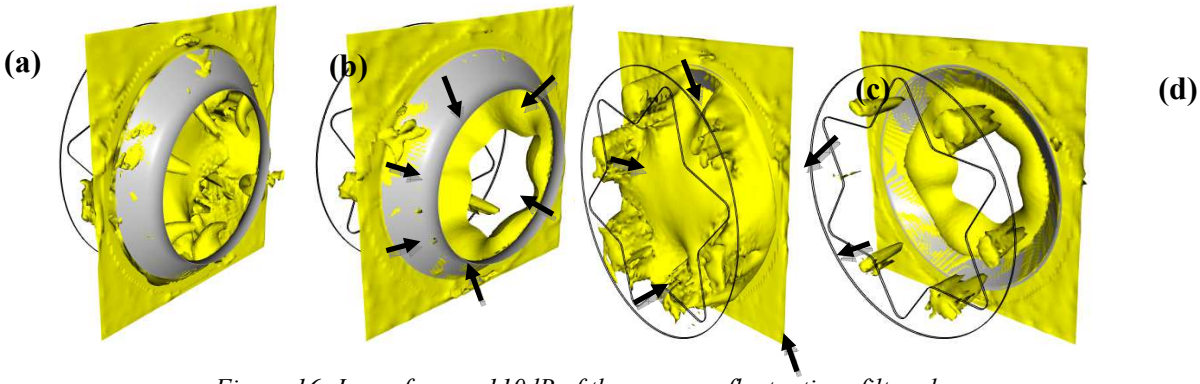

Figure 16: Isosurface p=110dB of the pressure fluctuations filtered around the BPF.(a) and (c) conf. C; (b) and (d): conf. C_{opt}.

CONCLUSIONS

In this paper, the effect of a flow obstruction on the fan blade passing frequency noise is investigated. Some experiments are performed on the CETIM aeroacoustics bench for various configuration and obstruction positions. For an optimal position, it is seen that the obstruction reduces the BPF noise by 10-13 dB. Transient, explicit and compressible CFD/CAA simulations are performed in order to validate the numerical approach and to evaluate the potential of a digital approach to optimize a complex fan noise problem. Comparisons between the experiments and the simulations are in a very satisfying agreement for the various configurations and in particular the fan noise and the heat exchanger effects are correctly modelled. Furthermore, calculations performed at various obstruction angles show that the simulations capture the correct effect of the obstruction position on the BPF noise indicating that this digital approach could be considered in addition, or in replacement, to the current experimental approach. It can also be emphasized that real and complex systems such a complete under-hood with exchanger, grill, engine can be modelled and the effect of obstructions mounted in real environment quantified. The simulation is also used to have an insight on the noise reduction mechanism and is shown to be related to a change in the flow topology and in the presence or not of coherent vortices in the system.

BIBLIOGRAPHY

[1] A. Gerard, A. Berry, P. Masson, Y. Gervais, "*Passive adaptive control of tonal noise from subsonic axial fans using flow control obstructions*", Fan Noise 2007 international conference, Paper 09, Lyon, France, **2007**

[2] Y. Goth, M. Besombes, C. Chassaignon, "*Fan Tonal Noise Reduction using Calibrated Obstructions in the Flow - An Experimental Approach*", Fan Noise 2012 International Conference, Senlis, France, **2012**

[3] K.D. Ih, S.R. Shin, S. Senthooran, B. Crouse and D.M. Freed, "*Activities of Digital Wind Noise Testing Process for Virtual Prototype Development*", 2009 JSAE Annual Congress, 203-20095476

[4] D.K Lee, F. Pérot, M.S. Kim, D.M. Freed, K.D. Ih, "*Aeroacoustics Predictions of Automotive HVAC Systems*", SAE World Congress, SAE 2011-01-0415, **2011**

[5] F. Pérot. M.S. Kim, D.M. Freed, D.K Lee, K.D. Ih, M.S. Kim, "*Direct aeroacoustics prediction of ducts and vents noise*", 16th AIAA/CEAS Aeroacoustics Conference, AIAA 2010-3724, Stockholm, Sweden, **2010**

[6] F. Pérot, M.S. Kim, S. Moreau, and D. Neal, "*Investigation of the Flow Generated by anAxial 3-Blade Fan*", 13th ISROMAC Conference, 2010-082, onolulu, Hawaii, April **2010**

[7] F. Pérot, M.S. Kim, S. Moreau, M. Henner, and D. Neal, "*Direct Aeroacoustics Prediction of a Low Speed Axial Fan*", 16th AIAA/CEAS Aeroacoustics Conference, AIAA-2010-3887, Stockholm, Sweden, June **2010**

[8] F. Pérot, M.S. Kim,K. Wada, K. Norisada, M. Kitada, S. Hirayama, M. Sakai, S. Imahigasi, N. Sasaki "*HVAC blower aeroacoustics predictions based on the lattice Boltzmann method*", AJK Conference, AJK2011-23018, Hamamatsu, Japan, **2011**.

[9] A. Laffite, F. Pérot, "*Investigation of the Noise Generated by Cylinder Flows Using a Direct Lattice-Boltzmann Approach*", AIAA 2009-3268, **2009**.

[10] G.A. Brès, F. Pérot, D. Freed, "*Properties of the Lattice-Boltzmann Method for Acoustics*", AIAA 2009-3395, **2009**.

[11] S. Marié, D. Ricot, and P. Sagaut, "*Comparison Between Lattice Boltzmann Method and Navier–Stokes High Order Schemes for Computational Aeroacoustics*", J. Comp. Physics, Vol. 228 #4 pp. 1056-1070, **2009**.

[12] U. Frisch, B. Hasslacher and Y. Pomeau, "*Lattice-gas Automata for the Navier-Stokes Equations*" Phys. Rev. Lett., Vol. 56, **1986**, pp.1505-1508.

[13] P. Bhatnagar, E. Gross,M. Krook, "*A model for collision processes in gases. I. small amplitude processes in charged and neutral one-component system*", Pys. Rev., vol.94, pp.511-525, **1984**.

[14] S. Chapmanand T. Cowling, "*The Mathematical Theory of Non-Uniform Gases*", Cambridge University Press, **1990**.

[15] X. Shanand, H. Chen, "*Lattice Boltzmann model for simulating flows with multiple phases and components*", Phys. Rev. E, 47, 1815-1819, **1983**.

[16] Y. Li, R. Shock, R. Zhang, and H. Chen, "*Numerical Study of Flow Past an Impulsively Started Cylinder by Lattice Boltzmann Method*", J. Fluid Mech., Vol. 519, pp. 273-300, **2004**.

[17] H. Chen, S. Orszag, I. Staroselsky, S. Succi, "*Expanded Analogy between Boltzmann Kinetic Theory of Fluid and Turbulence*", J. Fluid Mech., Vol. 519, pp. 301-314, **2004**.

[18] H. Chen, C. Teixeira, K. Molvig, "*Realization of Fluid Boundary Conditions via Discrete Boltzmann Dynamics*" Intl J. Mod. Phys. C, Vol. 9 (8), pp. 1281-1292, **1998**.

[19] H. Chen, "*Volumetric Formulation of the Lattice Boltzmann Method for Fluid Dynamics: Basic Concept*", Phys. Rev. E, Vol. 58, pp. 3955-3963, **1998**.

[20] G.Tabor, A.D. Gosman and R. Issa, "*Numerical Simulation of the Flow in a Mixing Vessel Stirred by a Rushton Turbine*" IChemE Symp Ser 140, 25-34, **1996**.

[21] Ph. Daskapoulous and C.K. Harris "*Three dimensional CFD simulations of Turbulent Flow in Baffled Stirred Tanks*" I ChemE Symp Ser 140, 1-13, 1996.

[22] H. Chen, "*Matching MRF Surfels for Sliding Mesh*", Exa Corporation Internal Notes, **2005**

[23] J.Hoch, "*Rotating Reference Frames in PowerFLOW*", Exa Corporation Internal Memorandum, **2004**

[24] R. Zhang, X. Shan and H. Chen, "*Efficient Kinetic Method for fluid simulation beyond Navier-Stokes equation*", Phys. Rev. E, 74, 046703, **2006**.

[25] M.S. Kim, F. Pérot, M. Meskine, "*Aerodynamics and acoustics predictions of the 2-blade NREL wind turbine using a Lattice Boltzmann Method*", 14th International Symposium on Rotating MAChinery (ISROMAC), February 2012

[26] F. Pérot, A. Mann, M.S. Kim, E. Fares, "*Advanced Noise Control Fan Direct Aeroacoustics Predictions using a Lattice-Boltzmann Method*", Submitted to the 17th AIAA/CEAS Aeroacoustics Conference, June **2012**, Colorado Springs, USA

[27] S. Magne, *Private Communication*, 2011.

[28] A. Gérard, A. Berry, P. Masson, "*Active control of tonal noise from subsonic axial fan. Part 2 : Active control simulations and experiments in free field*", Journal of Sound and Vibration, vol. 288, no 4-5, p. 1077–1104, **2005**.

[29]G. Fournier, G. Huard, J. Pérucchini, "*Noise reduction of fans by control of flow distortion*", Inter Noise **1994**, Yokohama, Japan

[30] C. Polacsek, F. Desbois-Lavergne, "*Fan interaction noise reduction using a wake generator: experiments and computational aeroacoustics*", Journal of Sound and Vibration, vol. 265, no 4, pp. 725-743, **2003**.